# Quiet time response of ionosphere over Nepal

**Drabindra Pandit***

*Department of Physics, St. Xavier's College, Maitighar, Kathmandu, Nepal.

**Abstract:** This study attempts to characterize the ionospheric behavior over Nepal during quiet periods by studying ionospheric total electron content in 2009 and 2014 utilizing ground-based GPS data from the station GRHI (Gorahi). The GPS receiver and satellite pseudorange measurement is used to compute the VTEC. Our study shows in the quietest day of January 12, 2009, at the minimum time of solar cycle 24, and January 19, 2014, during the highest phase of solar cycle, a flat curve with a slight peak in the diurnal TEC of around 12 and 28 TECU. In 2009, there was no equinoctial asymmetry; nevertheless, in 2014, spring VTEC was higher than autumn VTEC. The plot reveals the highest VTEC in 2009 was between 10 and 30 TECU, and it spreads roughly from 7.75 to 18.75 LT. In 2014, the maximum VTEC was between 20 and 120 TECU, and it spreads from 8.75 to 17.90 LT. Spring had the highest value and winter the lowest in 2009, but, in 2014 summer had the lowest value and spring the highest value of TEC. The results of this study advance our understanding of ionospheric physics and offer important new perspectives on the evolution of the ionospheric layer over Nepal and other comparable regions.

**Keywords**: Quiet time; Ionosphere; Total electron content (TEC).

## Introduction

The ionosphere plays a crucial role in space weather phenomena. Research in this area can help in monitoring and predicting space weather events, such as solar flares and geomagnetic storms, which can have impacts on satellite operations, communication systems, and power grids. Investigating the ionosphere is essential for understanding how radio waves propagate through it. This knowledge is crucial for optimizing communication systems, including long-range radio communication and the functioning of high-frequency (HF) communication systems. Studying the ionosphere above Nepal may provide insights into the behavior of the ionosphere in the region, contributing to the broader understanding of magnetospheric processes.

Solar extreme ultraviolet (EUV) ionization causes TEC to peak at local noon, while recombination causes it to decline at night [1, 2]. Due to variations in the solar zenith angle and neutral composition, TEC is typically larger during equinoxes than during solstices [3, 4]. Winter TEC is higher than summer TEC in several mid-latitude zones, which may be caused by variations in the $[O]/[N_2]$ ratio [5].

Due to fountain effect dynamics, the equatorial ionization anomaly (EIA) produces two TEC peaks at around ±15° geomagnetic latitude [6]. This peak TEC is affected by electric fields and neutral wind [7]. Polar cap patches and auroral dynamics add variability even in quiet periods were studied [8]. In 1998 Mannucci et al.[9] noted that TEC and solar flux are highly correlated and ionization rises with increased of solar activity. Thermospheric winds, tides, and electric fields are the main factors influencing TEC fluctuations[10]. The TEC distribution is changed by neutral winds, which move plasma along magnetic field lines [11]. At the diurnal and semi-diurnal timeframes, TEC is modulated by atmospheric tides from the lower atmosphere [12,13]. Through E×B drifts, the EEJ affects low-latitude TEC even in quiet periods [14]. High-resolution TEC estimates can be obtained using dual-frequency GPS/GLONASS receivers [15]. Giving comparable profiles of electron density [16]. Global TEC/climatology data are provided by COSMIC, CHAMP, and Swarm [17] which are commonly employed, although it understates low-latitude quiet-time TEC [18].

***Author for correspondence***: Drabindra Pandit, Department of Physics, St. Xavier's College, Maitighar, Kathmandu, Nepal.
Email: drabindra@sxc.edu.np; https://orchid.org/0000-0002-1955-8499
Received: 6 July, 2025; Received in revised form: 9 Sept, 2025; Accepted: 14 Sept, 2025.
Doi: https://doi.org/10.3126/sw.v19i19.95735

NeQuick model adaptable for quiet-time TEC with solar flux inputs [19].TIEGCM (Thermosphere-Ionosphere-Electrodynamics GCM) simulates quiet-time TEC with neutral dynamics [20]. Even during quiet periods, unexplained TEC fluctuations persist [21]. More studies needed to isolate pure quiet-time behavior from residual storm effects [22]. Emerging AI-based models (e.g., LSTM networks) show promise in quiet-time TEC forecasting [23]. Maute et al. (2016)[24] examines tidal influences on ionospheric variability. Jones Jr. et al. (2018) analyzed wind-induced plasma transport effects[26]. Rishbeth (1998) explains how neutral composition changes affect ionospheric electron density[11]. Fuller-Rowell (1996) discusses seasonal variations in $O/N_2$ ratio[26]. In this research, variation in total electron content during quiet time of minimum and maximum of solar cycle 24 is discussed. Section 2 discusses the dataset and methodology, the results and discussion are elaborated in section 3, and 4 summarizes the outcomes of the paper.

**Dataset and Methodology**

The ten quietest days of each month of year 2009 and 2014 are taken from International Service of Geomagnetic indices (ISGI) using website: https://isgi.unistra.fr. The order number of the ten quietest days of the month is represented by the Q-Days values, Q1–Q10. To reduce geomagnetic contamination, quiet days were chosen based on predetermined parameters ($Kp \leq 2$, $Ap \leq 7$) (Mendillo, 2006) whereas for disturbed day threshold value Kp and Ap is: $Kp \geq 5$; $Ap \geq 32$[27]. Then the GPS data for each quiet day is used to calculate TEC.

The columnar electron density throughout the route from the reception to the satellites is known as total electron content, or TEC. The TEC is computed as

$$TEC = \int N_e(h)\, dh \qquad (1)$$

where, $N_e$ is electron density, $R$ is receiver altitude and $S$ satellite altitude.

The traditional method for processing GPS pseudorange measurements is used to calculate Vertical TEC (VTEC) [28,29]. The dual frequency GPS receiver, which operates in the two L-bands at frequencies of $f_1$-1575.42 MHz and $f_2$-1227.60 MHz, provides measurements of the carrier phase and pseudo-range. Hofmann-Wellenhof et al. (1992)[28] state that the TEC is calculated using the carrier phase and the $L_1$ and $L_2$ pseudo-ranges. TEC is calculated using the pseudo-range and phase data in the following formula:

$$TEC = \frac{1}{40.3}\left(\frac{{f^2}_1 {f^2}_2}{{f^2}_2 - {f^2}_1}\right)(P_1 - P_2) \qquad (2)$$

Where, $P_1$ and $P_2$ are the pseudo-ranges for frequencies $f_1$ and $f_2$, respectively.

Slanted TEC (STEC), which is the entire electron content of the ionosphere as measured along the ray route from the satellite to the receiver, needs to be transformed into vertical TEC (VTEC) using the formula (Titheridge, 1972)[30].

$$VTEC = (STEC - B_s - B_u)\sqrt{1 - \frac{R_E \cos\epsilon}{(R_E+h)^2}} \qquad (3)$$

where $B_s$ and $B_u$ are the biases of satellite instruments and receivers, respectively, $\epsilon$ is the satellite's elevation angle, and $R_E$ = 6371 km is the Earth's mean radius.

The GPS data for this study is taken from GRHI station from Nepal because it consists of continuous data which is useful for this study. The table 1 shows the geophysical location of the station of which data is used in this study. The data is downloaded from the website freely for any user http://www.unavco.org. These data are accessible in the widely used ASCII (American Standard Code for Information Interchange) format known as RINEX (Receiver Independent Exchange) v2.1. This data has a 15-minute temporal resolution. Software created by Rolland Fleury (Lab-STICC, UMR 6285, Institut Mines-Télécom Atlantique, site de Brest, France; accessible at http://www.girgea.org, July 19, 2018) is then used to process the raw data. The necessary VTEC for plotting and analyzing is obtained by running on a Windows operating system.

**Results and Discussion**

**Diurnal variation of VTEC**

Figure 1 shows the diurnal plot of VTEC at GRHI GPS station of Nepal during quietest day of January 2009 and 2014 ie on 12 January 2009 (left) and on 19 January 2014

**Table 1: Geophysical location of GPS station used.**

| ID | Location | Geographical lat. and log. | Geomagnetic lat. and lon. | Dip latitude | Local time |
|---|---|---|---|---|---|
| GRHI | Ghorahi, Nepal | 27.95°N; 82.49° E | 18.94°N; 156.82°E | 44.25°N | UT + 5.75 hour |

(right). The plot indicates the maximum value of VTEC on 12 January 2009 is 13.60 TECU at 8.63 UT (14.08 LT) and the maximum value of VTEC on 19 January 2014 is 29.30 TECU at 5.88 UT (11.63 LT). The sunrise and sunset time on 12 January 2009 were 1.06 UT (6.82 LT); 11.56 UT (17.31 LT) with length of sunshine approximately 10.5 hour and on 19 January 2014 was 1.36 UT (7.11 LT); 11.99 UT (17.74 LT) with length of sunshine approximately 10.5 hour respectively. The VTEC of Nepal exhibit strong diurnal pattern, the peaks during mid-day at (11:00-14:00) LT, minima during pre-sunrise (04:00-6:00) LT and nighttime (20:00–02:00 LT). This pattern results from ionization caused by solar radiation during the day and recombination activities throughout the night. The enhanced photoionization from solar UV and X-ray radiation causes VTEC to rise after sunrise when solar zenith angles are at their lowest, and falls at night when ionization diminishes (29, 30). In 2021, Pandit et al, noted flat curve with minor peaks in diurnal pattern of 2009 and dome shaped curve in 2014 maximum period of solar cycle 24 over Nepal. The modulation of plasma transport in the ionosphere by neutral winds and atmospheric tides, including the migrating diurnal tide, affects TEC changes [33, 34]. These winds have the ability to shift the ionospheric plasma's altitude, which alters the electron density [35].

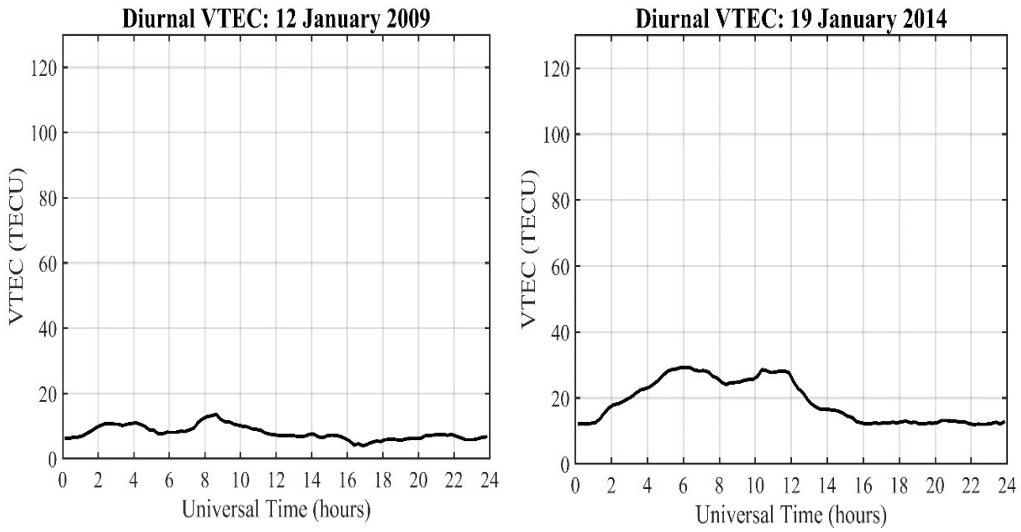


**Figure 1: Diurnal VTEC profile of quiet day of 12 January 2009 (left) and 19 January 2014 (right).**

**Monthly variation of VTEC**

The plots in the Figure 2 (i-xii) left represents how the diurnal VTEC from January to December in 2009 and Figure 2 (i-xii) right represents diurnal VTEC from January to December in 2014. The table 2 summarizes the maximum and minimum value of VTEC in different month of 2009 and 2014. The peak values in VTEC varies from 19.13 TECU (December 13.88 LT) to 31.38 TECU (March 15.88 LT) and the minimum VTEC it varies from 11.58

TECU (January 8.63 LT) to 20.58 TECU (April 13.88 LT) in 2009. In year 2014 the maximum VTEC varies from 120.45 TECU (March 14.13 LT) to 45.81 TECU (January 12.88) and the minimum VTEC varies from 76.29 TECU (March 14.13 LT) to 23.55TECU (July 16.13 LT). In general, from the plots, it seems that the TEC over Nepal exhibits notable monthly variations, peaking around the equinoxes (March-April; September-October) and lowest during the solstices (November, December, January, February, May, June, July, August). Due to equinoctial asymmetry, March-April has a slightly higher TEC than September-October. Decrease in solar EUV flux, in the winter solstice (November, December, January, February) has the lowest TEC. Moderate VTEC at the summer solstice (May, June, July, August) is impacted by neutral wind dynamics. But November of 2014 winter anomaly has noticed. Pre-reversal enhancements in the evening peak are noticed only in February, March, October, November and December in 2014 but not it is identified in 2009. Double diurnal peaks are obtained in February, march, August and September of 2014. Similar result was obtained by Pandit et al., (2021)[32] in study the climatology of ionosphere over Nepal. Enhanced ionization and decreased recombination rates are the results of wintertime increases in atomic oxygen (O) relative to molecular nitrogen ($N_2$) [11]. Atomic oxygen is moved from the summer to the winter hemisphere by meridional winds. Dissociative recombination causes less electron loss when molecular nitrogen ($N_2$) is lower [26]. In winter, recombination is decreased by meridional winds that carry plasma along magnetic field lines to higher elevations [36]. The distribution of plasma is changed by the modification of neutral winds by atmospheric tides and planetary waves. Over the winter, downwelling lowers $N_2$ and raises O density [24].

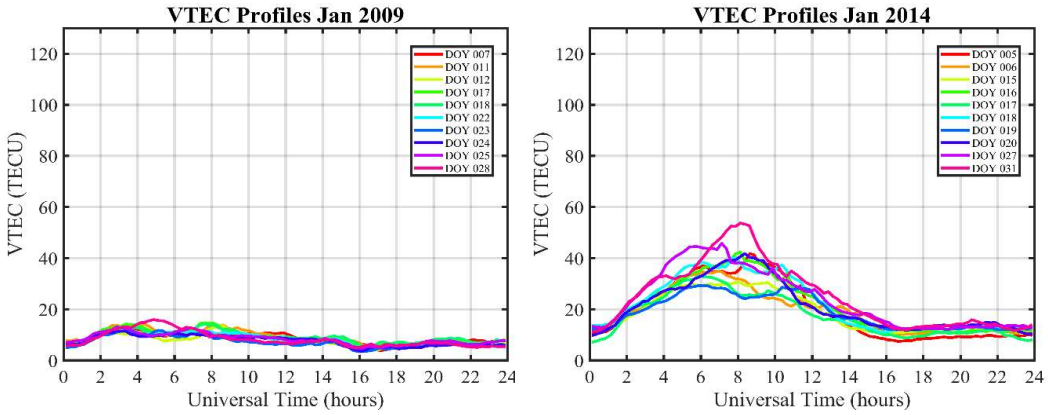


(i)

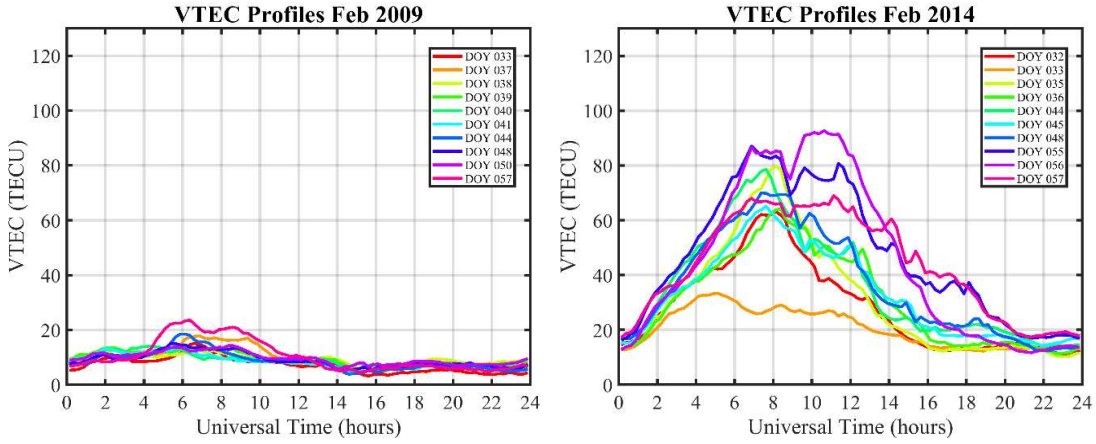


(ii)

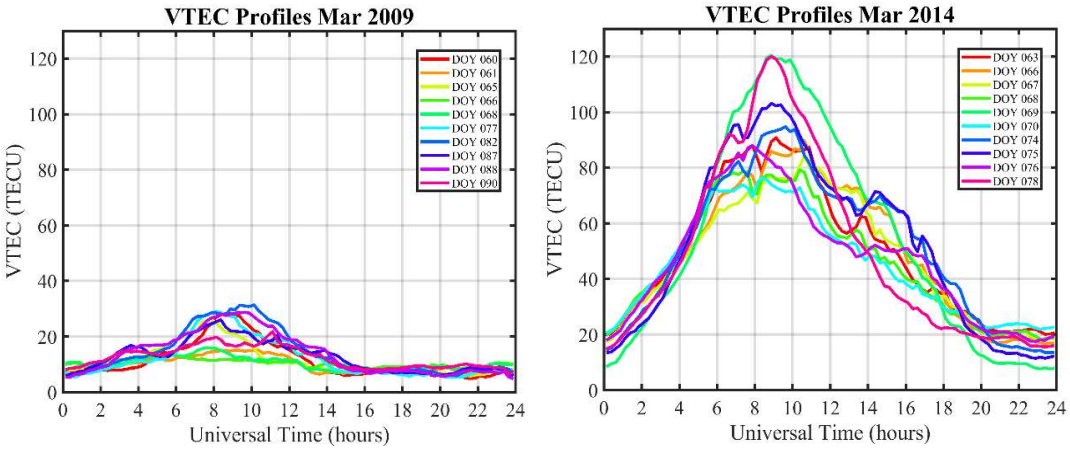
VTEC Profiles Mar 2009
VTEC (TECU)
Universal Time (hours)
DOY 060
DOY 061
DOY 065
DOY 066
DOY 068
DOY 077
DOY 082
DOY 087
DOY 088
DOY 090
VTEC Profiles Mar 2014
VTEC (TECU)
Universal Time (hours)
DOY 063
DOY 066
DOY 067
DOY 068
DOY 069
DOY 070
DOY 074
DOY 075
DOY 076
DOY 078

(iii)

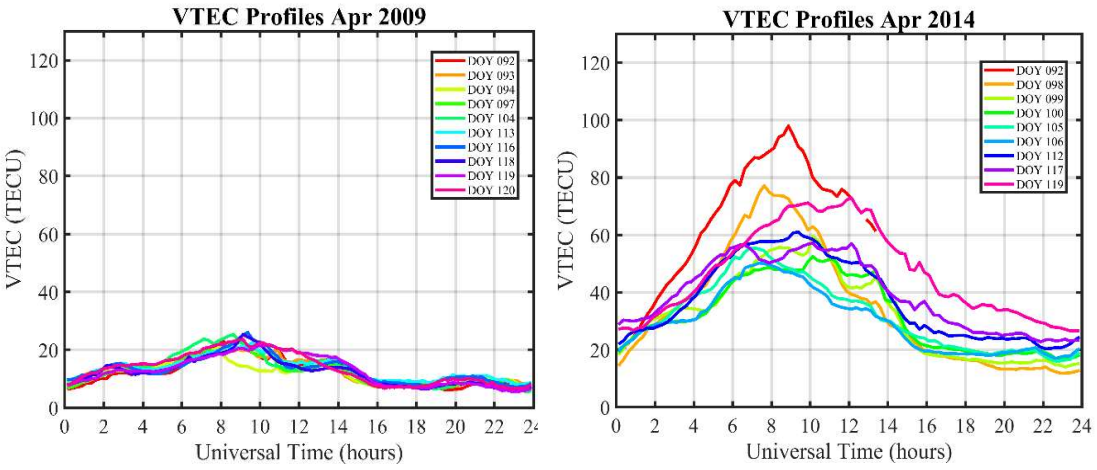
VTEC Profiles Apr 2009
VTEC (TECU)
Universal Time (hours)
DOY 092
DOY 093
DOY 094
DOY 097
DOY 104
DOY 113
DOY 116
DOY 118
DOY 119
DOY 120
VTEC Profiles Apr 2014
VTEC (TECU)
Universal Time (hours)
DOY 092
DOY 098
DOY 099
DOY 100
DOY 105
DOY 106
DOY 112
DOY 117
DOY 119

(iv)

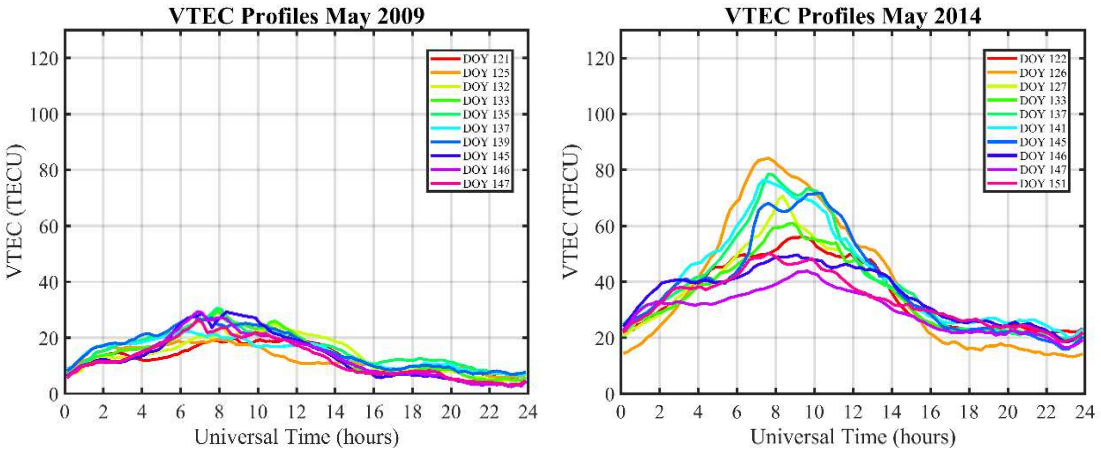
VTEC Profiles May 2009
VTEC (TECU)
Universal Time (hours)
DOY 121
DOY 125
DOY 132
DOY 133
DOY 135
DOY 137
DOY 139
DOY 145
DOY 146
DOY 147
VTEC Profiles May 2014
VTEC (TECU)
Universal Time (hours)
DOY 122
DOY 126
DOY 127
DOY 133
DOY 137
DOY 141
DOY 145
DOY 146
DOY 147
DOY 151

(v)

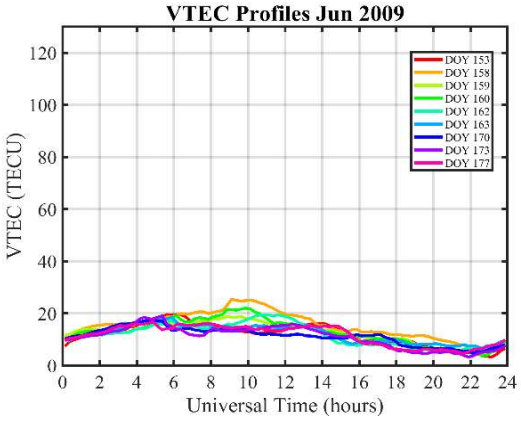
VTEC Profiles Jun 2009
VTEC (TECU)
Universal Time (hours)
DOY 153
DOY 158
DOY 159
DOY 160
DOY 162
DOY 163
DOY 170
DOY 173
DOY 177

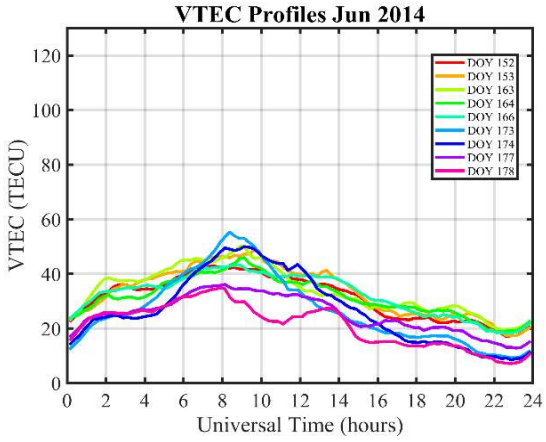
VTEC Profiles Jun 2014
VTEC (TECU)
Universal Time (hours)
DOY 152
DOY 153
DOY 163
DOY 164
DOY 166
DOY 173
DOY 174
DOY 177
DOY 178

(vi)

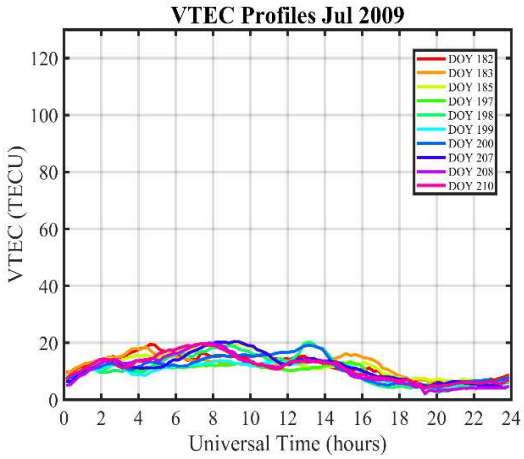
VTEC Profiles Jul 2009
VTEC (TECU)
Universal Time (hours)
DOY 182
DOY 183
DOY 185
DOY 197
DOY 198
DOY 199
DOY 200
DOY 207
DOY 208
DOY 210

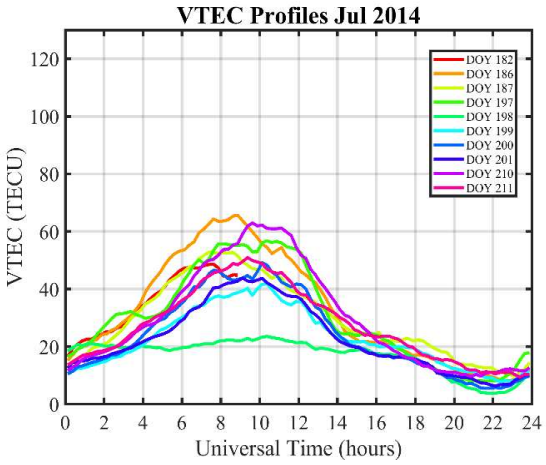
VTEC Profiles Jul 2014
VTEC (TECU)
Universal Time (hours)
DOY 182
DOY 186
DOY 187
DOY 197
DOY 198
DOY 199
DOY 200
DOY 201
DOY 210
DOY 211

(vii)

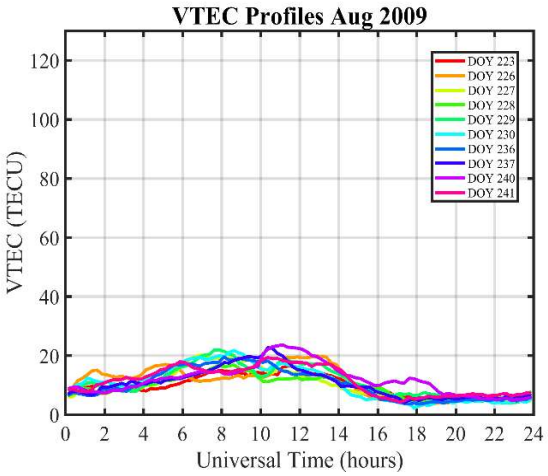
VTEC Profiles Aug 2009
VTEC (TECU)
Universal Time (hours)
DOY 223
DOY 226
DOY 227
DOY 228
DOY 229
DOY 230
DOY 236
DOY 237
DOY 240
DOY 241

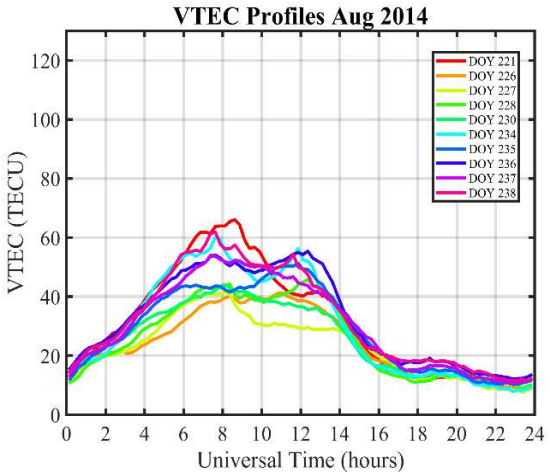
VTEC Profiles Aug 2014
VTEC (TECU)
Universal Time (hours)
DOY 221
DOY 226
DOY 227
DOY 228
DOY 230
DOY 234
DOY 235
DOY 236
DOY 237
DOY 238

(viii)

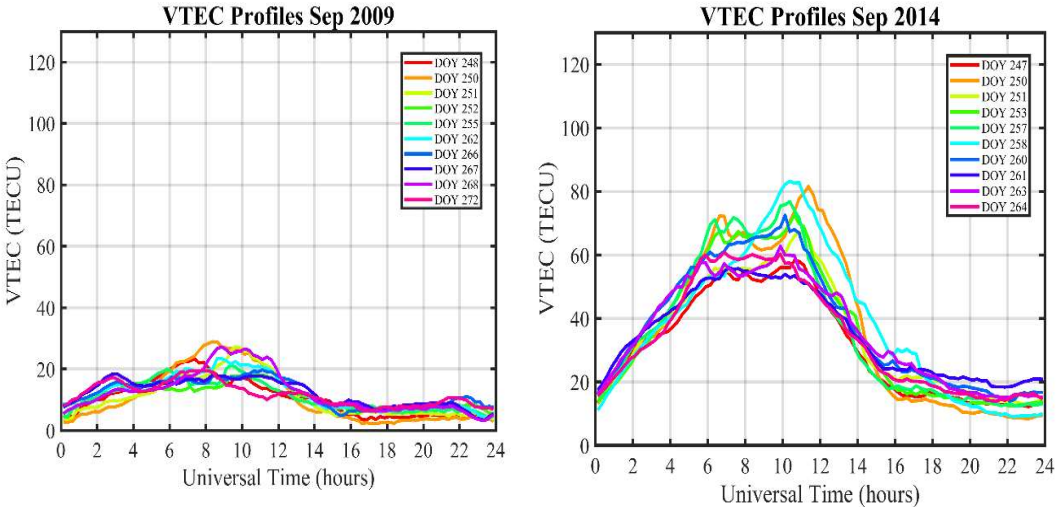
VTEC Profiles Sep 2009
VTEC (TECU)
Universal Time (hours)
DOY 248
DOY 250
DOY 251
DOY 252
DOY 255
DOY 262
DOY 266
DOY 267
DOY 268
DOY 272
VTEC Profiles Sep 2014
VTEC (TECU)
Universal Time (hours)
DOY 247
DOY 250
DOY 251
DOY 253
DOY 257
DOY 258
DOY 260
DOY 261
DOY 263
DOY 264

(ix)

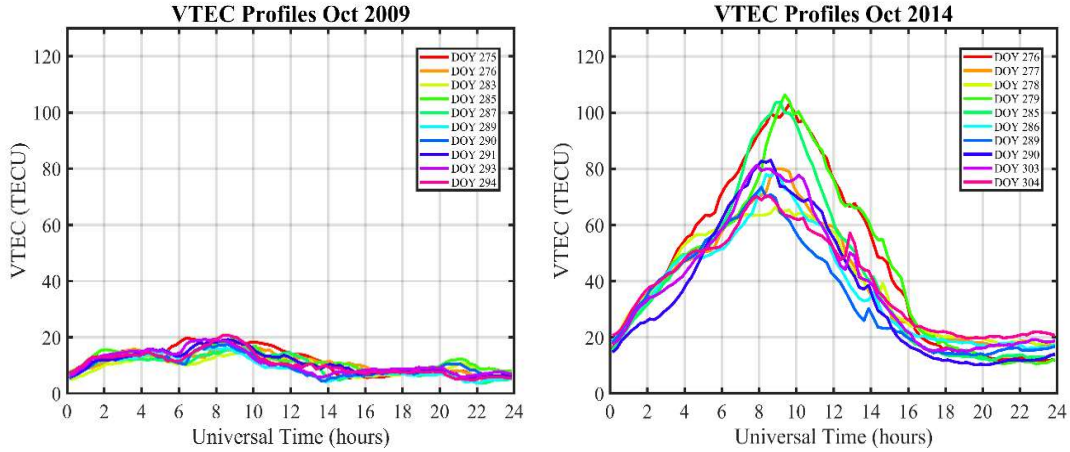
VTEC Profiles Oct 2009
VTEC (TECU)
Universal Time (hours)
DOY 275
DOY 276
DOY 283
DOY 285
DOY 287
DOY 289
DOY 290
DOY 291
DOY 293
DOY 294
VTEC Profiles Oct 2014
VTEC (TECU)
Universal Time (hours)
DOY 276
DOY 277
DOY 278
DOY 279
DOY 285
DOY 286
DOY 289
DOY 290
DOY 303
DOY 304

(x)

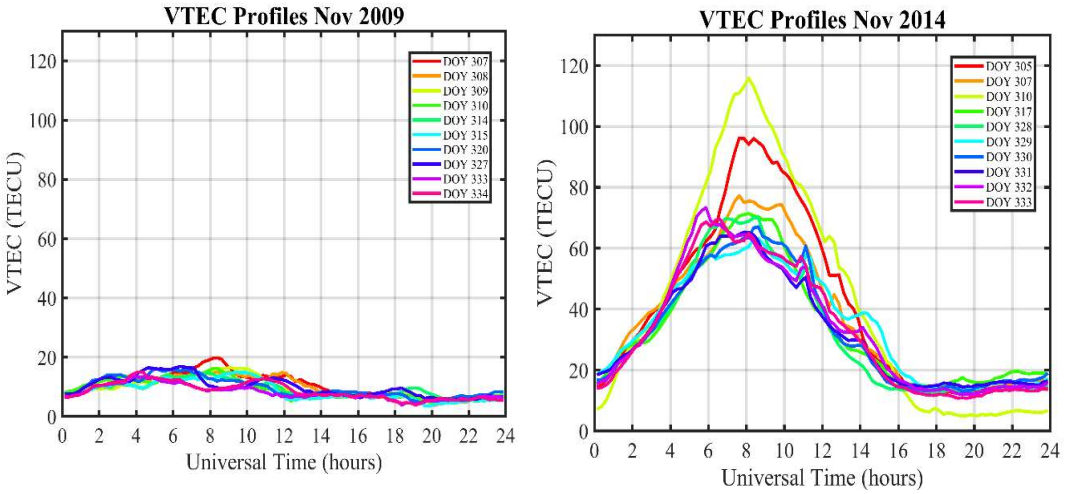
VTEC Profiles Nov 2009
VTEC (TECU)
Universal Time (hours)
DOY 307
DOY 308
DOY 309
DOY 310
DOY 314
DOY 315
DOY 320
DOY 327
DOY 333
DOY 334
VTEC Profiles Nov 2014
VTEC (TECU)
Universal Time (hours)
DOY 305
DOY 307
DOY 310
DOY 317
DOY 328
DOY 329
DOY 330
DOY 331
DOY 332
DOY 333

(xi)

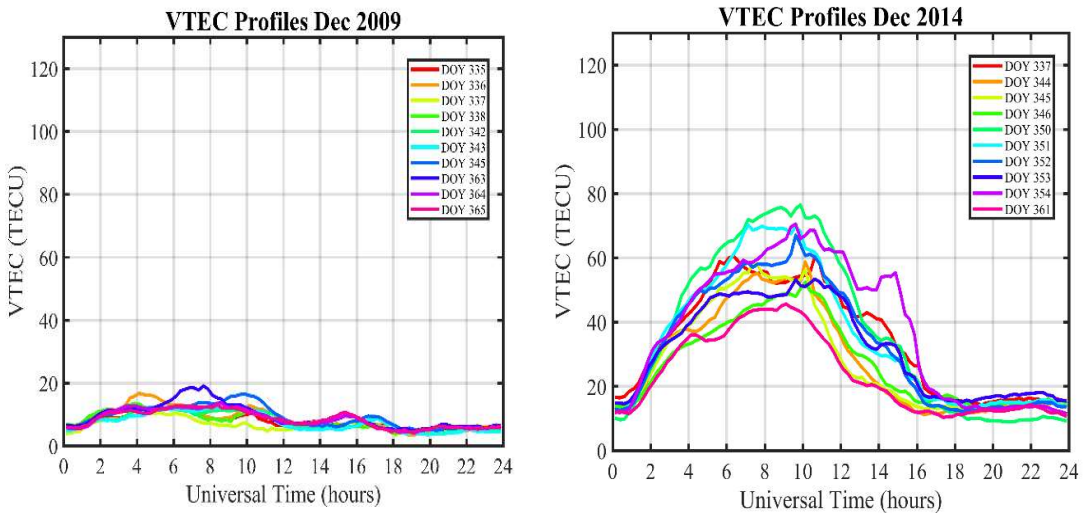


(xii)

**Figure 2: (i-xii) Left panels from the top to bottom shows monthly profile quiet days variation of VTEC in the month of January to December in 2009 and right panels from the top to bottom shows variation of VTEC in the of month January to December in 2014.**

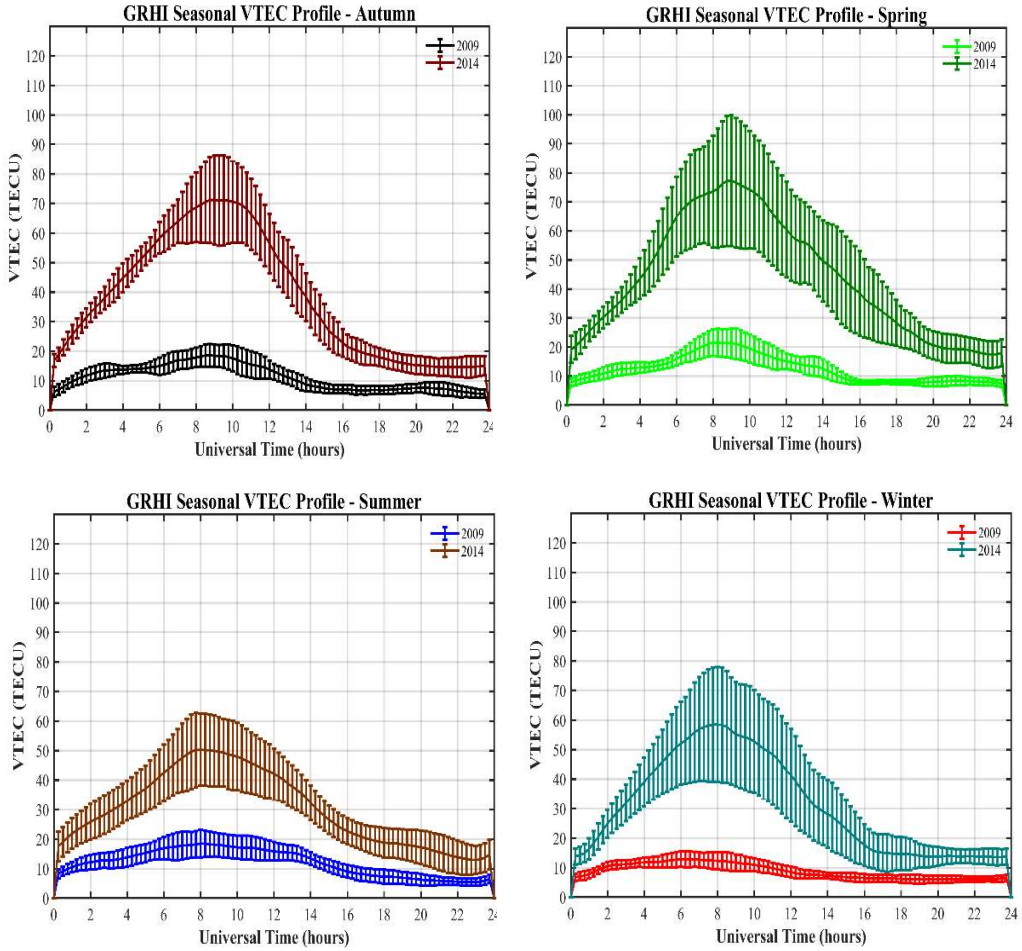


**Figure 3: Illustrating the seasonal variation of VTEC in year 2009 and 2014 (top left: autumn; top right: spring; bottom left: summer and bottom right: winter). The black/red, green/dark green, blue/brown, red/cyan with respective error bar represents average VTEC for 2009 and 2014 of all the quiet days of the respective season.**

**Table 2: The maximum and minimum VTEC in different month of 2009 and 2014.**

| Year | Month | Day of Year | Max. VTEC (TECU) | Local time (UT+5.75) hours | Day of Year | Min. VTEC (TECU) | Local time (UT+5.75) hours |
|---|---|---|---|---|---|---|---|
| 2009 | Jan. | 28 | 15.93 | 10.63 | 24 | 11.52 | 8.63 |
| | Feb. | 44 | 18.53 | 11.88 | 38 | 12.70 | 12.63 |
| | Mar. | 82 | 31.38 | 15.88 | 66 | 13.70 | 11.38 |
| | Apr. | 116 | 26.00 | 15.13 | 93 | 20.58 | 13.88 |
| | May | 135 | 30.56 | 13.63 | 125 | 19.26 | 13.63 |
| | Jun. | 158 | 25.49 | 14.88 | 170 | 17.25 | 10.63 |
| | Jul. | 207 | 20.45 | 14.88 | 197 | 13.42 | 21.13 |
| | Aug. | 240 | 23.69 | 16.88 | 228 | 16.90 | 14.38 |
| | Sep. | 250 | 28.92 | 14.13 | 252 | 18.42 | 16.13 |
| | Oct. | 294 | 20.77 | 14.38 | 283 | 14.30 | 15.13 |
| | Nov. | 307 | 19.76 | 14.13 | 333 | 13.39 | 9.63 |
| | Dec. | 363 | 19.13 | 13.38 | 337 | 11.56 | 9.88 |
| 2014 | Jan. | 27 | 45.81 | 12.88 | 19 | 29.30 | 11.63 |
| | Feb. | 56 | 92.66 | 16.38 | 33 | 33.37 | 10.88 |
| | Mar. | 69 | 120.45 | 14.65 | 70 | 76.29 | 14.13 |
| | Apr. | 92 | 97.95 | 14.63 | 106 | 50.25 | 13.13 |
| | May | 126 | 84.20 | 13.38 | 147 | 43.92 | 15.38 |
| | Jun. | 173 | 55.33 | 14.13 | 178 | 34.86 | 13.63 |
| | Jul. | 186 | 65.64 | 14.63 | 198 | 23.55 | 16.13 |
| | Aug. | 221 | 66.09 | 14.38 | 226 | 41.24 | 16.63 |
| | Sep. | 258 | 83.18 | 16.13 | 261 | 56.01 | 12.88 |
| | Oct. | 279 | 106.28 | 15.13 | 178 | 66.41 | 14.63 |
| | Nov. | 310 | 115.82 | 13.88 | 329 | 63.13 | 14.38 |
| | Dec. | 350 | 76.56 | 15.63 | 361 | 45.65 | 14.88 |

**Seasonal variation of VTEC**

Figures 3 show the seasonal variation of VTEC in year 2009 and 2014 (top left: autumn; top right: spring; bottom left: summer and bottom right: winter). The black/red, green/dark green, blue/brown, red/cyan with respective error bar represents average VTEC for 2009 and 2014 for autumn, spring, summer and winter of all the quiet days of the respective season. The table 3 and 4 describes the seasonal profile of VTEC during 2009 and 2014. The highest VTEC has noticed in spring (March, 31.38 TECU, 15.88 LT), followed by summer (May, 30.56 TECU, 13.63 LT) then in autumn (September, 28.92 TECU, 14.13 LT) and the least is noticed during winter (February, 23.61, 12.08 LT) in 2009. The lowest minimum VTEC noticed in Autumn (October, 14.30 TECU, 15.13 LT), followed by spring (March, 13.70 TECU, 13.38 LT) then in summer (July, 13.42 TECU, 21.12 LT) and the least is noticed during winter (January, 11.52 TECU, 8.63 LT) respectively. In 2014 the highest VTEC is noted in spring (March, 120.45 TECU, 14.63 LT), followed by winter (November, 115.82 TECU, 13.88 LT) then in autumn (October, 106.28, 15.13 LT) and the least is noted in summer (May, 84.20 VTEC, 13.38 LT) and the lowest VTEC is noted highest in autumn (September, 58.20 VTECU, 16.38 LT), followed by spring (April, 50.25 TECU, 13.13 LT) then in winter (January, 29.30 TECU, 13.63LT) and least value is noted in summer (July, 23.35 TECU, 16.13) respectively. The general trends in the highest VTEC in spring is due to strong equatorial ionization anomaly (EIA) and comparatively lower value in autumn due to asymmetry in neutral wind circulation during this season. The lowest VTEC in winter is noticed due to minimal solar ionization. Summer time has a greater sun zenith angle than equinoxes, which lowers ionization efficiency even though daylight hours are longer. TEC is generally greater during equinoxes than during solstices because of differences in the sun zenith angle and neutral composition [3, 4].

**Seasonal variation of maximum VTEC**

Figure 4 Illustrating the maximum seasonal variation of VTEC with diurnal time in year 2009 (left) and 2014 (right) The plot shows in 2009 the maximum lies between 10 TECU to 30 TECU and spreads approximately from 7.75 LT to 18.75 UT whereas in 2014 the maximum VTEC lies between 20 TECU to 120 TECU and it spreads from 8.75 LT to 17.90 LT. In 2009 the highest value lies in Spring and lowest in winter but in 2014 the highest value lies in spring and lowest lies in summer.

**Yearly variation of VTEC**

Figure 5 shows year variation in VTEC in 2009 (black) and 2014 (red). The yearly profile in 2009 shows a flat curve of average VTEC whereas the parabolic nature of the curve is noticed 2014. Figure 6 demonstrates the quiet day variation maximum VTEC with respective time in year 2009 (top panel, i) and 2014 (bottom panel, ii). The x-axis represents

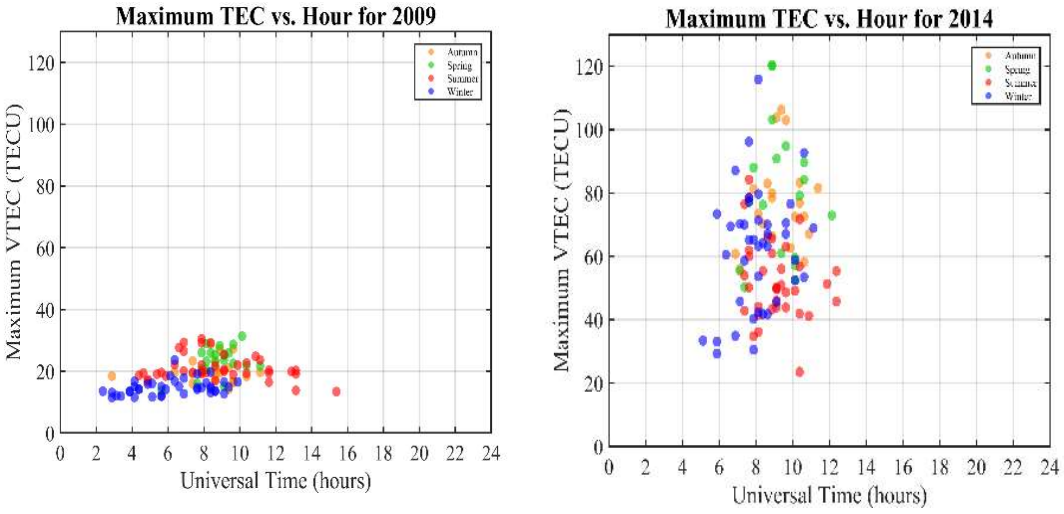


**Figure 4: Illustrating the maximum seasonal variation of VTEC in year 2009 (left) and 2014 (right).**

**Table 3: The maximum VTEC noted in different seasons of 2009 and 2014.**

| Year | Season | Month | Day of Year | Max. VTEC (TECU) | Local time (UT+5.75) hours |
|---|---|---|---|---|---|
| 2009 | Autumn | Sep. | 250 | 28.92 | 14.13 |
| | Spring | Mar. | 82 | 31.38 | 15.88 |
| | Summer | May | 135 | 30.56 | 13.63 |
| | Winter | Feb. | 57 | 23.61 | 12.08 |
| 2014 | Autumn | Oct. | 279 | 106.28 | 15.13 |
| | Spring | Mar. | 69 | 120.45 | 14.63 |
| | Summer | May | 126 | 84.20 | 13.38 |
| | Winter | Nov. | 310 | 115.82 | 13.88 |

**Table 4: The minimum VTEC noted in different seasons of 2009 and 2014.**

| Year | Season | Month | Day of Year | Min. VTEC (TECU) | Local time (UT+5.75) hours |
|---|---|---|---|---|---|
| 2009 | Autumn | Oct. | 283 | 14.30 | 15.13 |
| | Spring | Mar. | 66 | 13.70 | 13.38 |
| | Summer | Jul. | 197 | 13.42 | 21.12 |
| | Winter | Jan. | 24 | 11.52 | 8.63 |
| 2014 | Autumn | Sep. | 247 | 58.20 | 16.38 |
| | Spring | Apr. | 106 | 50.25 | 13.13 |
| | Summer | Jul. | 198 | 23.55 | 16.13 |
| | Winter | Jan. | 19 | 29.30 | 13.63 |

DOY, y-axis (left) time at which maximum VTEC occurs and y-axis (right) represents the maximum VTEC. The plot revels there is no asymmetry in VTEC in 2009 but its value is highest during spring than in autumn in 2014. More poleward meridional winds (from the summer to the winter hemisphere) raise plasma to greater heights, which lowers recombination losses. Upward plasma drift is enhanced by stronger migrating diurnal tides (DW1) [37]. Asymmetric tidal forcing is the cause of weaker poleward winds [12]. Dominant equatorward winds increase recombination ($O^+ + N_2 \rightarrow NO^+ + e^-$ loss) by pushing plasma downward. The $O/N_2$ ratio is reduced by decreasing atomic oxygen by

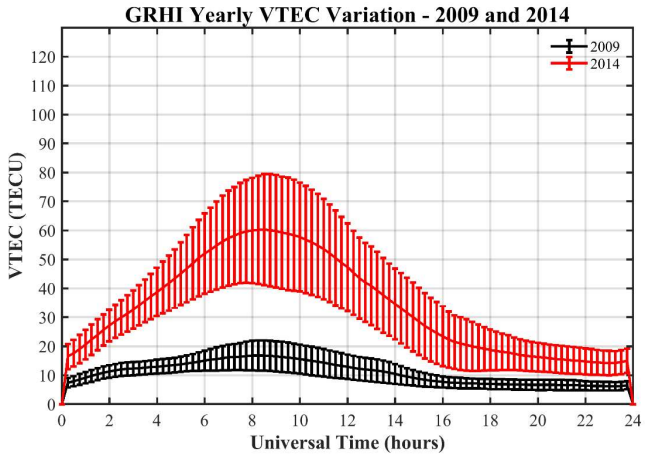


**Figure 6: Showing year variation in VTEC in 2009 (black) with error bar and 2014 (red) with error bar.**

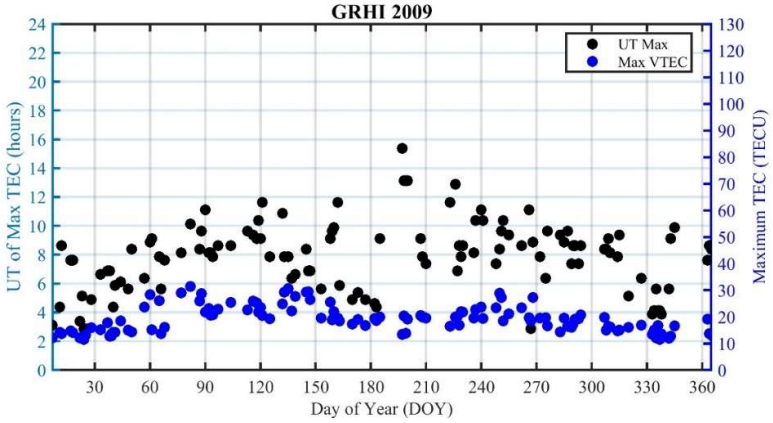


(i)

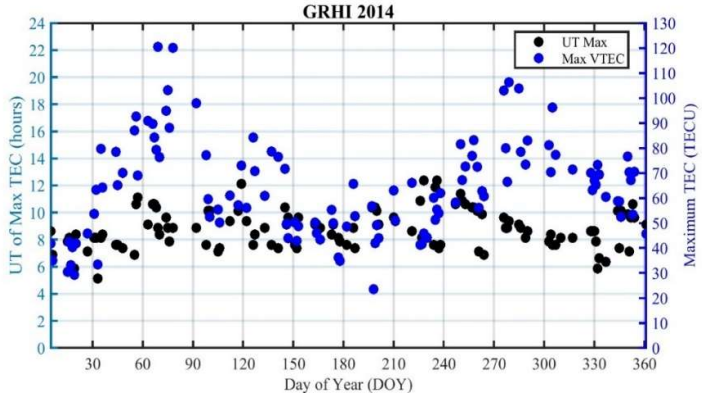


(ii)

**Figure 7: (i-ii) Demonstrating the quiet day variation maximum VTEC with respective time in year 2009 and 2014. The x-axis represents DOY, y-axis (left) time at which maximum VTEC occurs and y-axis (right) represents the maximum VTEC.**

residual summer hemisphere circulation [5].

**Conclusion**

This study presents quiet time variation of VTEC in 2009 and 2014 in ionosphere over Nepal by using data of the ground-based GPS data from the station GRHI (Gorahi). The TEC is calculated using pseudorange measurement between the GPS receiver and satellite. We draw some conclusions which are as follows:

- We observed flat curve with minor peak in diurnal TEC during quietest day of January 12, 2009 in the minimum period of solar cycle 24 and January 19, 2014 in the maximum period of solar cycle with their peak value is approximately 12 TECU and 28 TECU.
- Equinoctial asymmetry is not observed in 2009 but it is noted in 2014 in which spring VTEC is higher than autumn VTEC.
- The plot revels in 2009 the maximum lies between 10 TECU to 30 TECU and spreads approximately from 7.75 LT to 18.75 UT whereas in 2014 the maximum VTEC lies between 20 TECU to 120 TECU and it spreads from 8.75 LT to 17.90 LT. In 2009 the highest value lies in Spring and lowest in winter but in 2014 the highest value lies in spring and lowest lies in summer.
- Understanding the quiet time response of the ionosphere in this region has consequences for a variety of technology applications, including as satellite communications, navigation systems, and space weather forecasting.

**Data Availability Statement**

The data used in this study were obtained from the two websites. The quietest days of each month of the years 2009 and 2014 are taken from the International Service of Geomagnetic indices (ISGI) using the website: https://isgi.unistra.fr. The data for GPS TEC is downloaded from the website http://www.unavco.org, which is available freely to any user.

**Acknowledgements**

I would like to thank University Grant Commission for providing Small Research, Development and Innovation Programs Implementation (SRDIG 80/81-S&T-13) grant to do this research. Special thanks to the St. Xavier's College for providing facility in the college to carry out this research.

**References**

1. Afraimovich, E. L., Astafyeva, E. I., Oinats, A. V., Yasukevich, Yu. V. & Zhivetiev, I. V. 2008. GPS-derived TEC observations during quiet geomagnetic conditions. *Journal of Atmospheric and Solar-Terrestrial Physics*. **70**(11-12): 1542-1553. Doi: https://doi.org/10.1016/j.jastp.2008.05.010
2. Davies, K. 1990. Ionospheric radio (IEE Electromagnetic Waves Series, Vol. 31). Peter Peregrinus Ltd.
3. Rishbeth, H. & Garriott, O. K. 1969. Introduction to Ionospheric Physics. *Academic Press*.
4. Liu, H., Lühr, H., Watanabe, S., Köhler, W., Henize, V. & Visser, P. 2009. Zonal winds at 600-800 km altitude derived from CHAMP observations. *Annales Geophysicae*. **27**(3): 1207-1220. Doi: https://doi.org/10.5194/angeo-27-1207-2009
5. Balan, N., Shiokawa, K., Otsuka, Y., Kikuchi, T., Vijaya Lekshmi, D., Kawamura, S., Yamamoto, M. & Bailey, G. J. 2018. A physical mechanism of positive ionospheric storms at low latitudes and midlatitudes. *Scientific Reports*. **8**(1): 14666. Doi: https://doi.org/10.1038/s41598-018-33330-0
6. Appleton, E. V. 1946. Two anomalies in the ionosphere. *Nature*. **157**(3995): 691-693. Doi: https://doi.org/10.1038/157691a0
7. Mendillo, M. 2006. How the thermospheric circulation affects the ionospheric F2-layer. *Journal of Atmospheric and Solar-Terrestrial Physics*. **68**(8): 905–916.
8. Zou, S., Moldwin, M. B., Ridley, A. J., Nicolls, M. J., Coster, A. J., Thomas, E G. & Ruohoniemi, J. M. 2013. On the generation/decay of the storm-enhanced density plumes: Role of the convection flow and field-aligned ion flow. *Journal of Geophysical Research: Space Physics*. **118**(8): 5046-5059. Doi: https://doi.org/10.1002/jgra.50463
9. Mannucci, A. J., Wilson, B. D., Yuan, D. N., Ho, C. H., Lindqwister, U. J. & Runge, T. F. 1998. A global mapping technique for GPS-derived ionospheric total electron content measurements. *Radio Science*. **33**(3): 565-582. Doi: https://doi.org/10.1029/97RS02707
10. Abdu, M. A. 2016. Electrodynamics of ionospheric weather over low latitudes. *Geoscience Letters*. **3**(1): 11. Doi: https://doi.org/10.1186/s40562-016-0043-6
11. Rishbeth, H. 1998. How the thermospheric circulation affects the ionospheric F2-layer. *Journal of Atmospheric and Solar-Terrestrial Physics*. **60**(14): 1385-1402. Doi: https://doi.org/10.1016/S1364-6826(98)00062-5
12. Hagan, M. T., Demuth, H. B., Beale, M. H. & De Jesús, O. 2011. *Neural network design* .2nd edition, Martin Hagan.
13. Forbes, J. M., Zhang, X., Palo, S. E., Russell, J., Mertens, C. J. & Mlynczak, M. 2002. Troposphere-thermosphere tidal coupling as measured by the SABER instrument on TIMED during July–September 2002. *Geophysical Research Letters*. **29**(9): 1306.

Doi: https://doi.org/10.1029/2001GL014468

14. Fejer, B. G., Souza, J. R., Santos, A. S. & Costa Pereira, A. E. 2008. Climatology of F region zonal plasma drifts over Jicamarca. *Journal of Geophysical Research: Space Physics*. **113**(A12): A12311. Doi: https://doi.org/10.1029/2008JA013466
15. Ciraolo, L., Azpilicueta, F., Brunini, C., Meza, A. & Radicella, S. M. 2007. Calibration errors on experimental slant total electron content (TEC) determined with GPS. *Journal of Geodesy*. **81**(2): 111-120. Doi: https://doi.org/10.1007/s00190-006-0093-1
16. Reinisch, B. W. & Galkin, I. A. 2011. Global ionospheric radio observatory (GIRO). *Earth, Planets and Space*. **63**(4): 377-381. Doi: https://doi.org/10.5047/eps.2011.03.001
17. Lei, J., Thayer, J. P., Forbes, J. M., Sutton, E. K. & Nerem, R. S. 2007. Rotating solar coronal holes and periodic modulation of the upper atmosphere. *Geophysical Research Letters*. **34**(6): L06109. Doi: https://doi.org/10.1029/2006GL028764
18. Bilitza, D., Altadill, D., Truhlik, V., Shubin, V., Galkin, I., Reinisch, B. & Huang, X. 2017. International Reference Ionosphere 2016: from ionospheric climate to real-time weather predictions. *Space Weather*. **15**(2): 418-429.
19. Nava, B., Coïsson, P. & Radicella, S. M. 2008. A new version of the NeQuick ionosphere electron density model. *Journal of Atmospheric and Solar-Terrestrial Physics.* **70**(15): 1856-1862. Doi: https://doi.org/10.1016/j.jastp.2008.01.015.
20. Richmond, A. D., Ridley, E. C. & Roble, R. G. 1992. A thermosphere/ionosphere general circulation model with coupled electrodynamics. *Geophysical Research Letters*. **19**(6): 601–604. Doi: https://doi.org/10.1029/92GL00401.
21. Liu, L. & Watanabe, S. 2008. Climatology of quiet-time ionospheric variability. *Annales Geophysicae*. **26**(6): 1447-1461. Doi: https://doi.org/10.5194/angeo-26-1447-2008.
22. Astafyeva, E., Zakharenkova, I. & Förster, M. 2016. Ionospheric response to the 2015 St. Patrick's Day storm: A global multi-instrumental overview. *Journal of Geophysical Research: Space Physics*. **121**(10): 10,402-10,418. Doi: https://doi.org/10.1002/2015JA021629.
23. Habarulema, J. B., Okoh, D., McKinnell, L.-A., Cilliers, P., Ngwira, C. & Shiokawa, K. 2020. A neural network-based ionospheric model over Africa from constellation observing system for meteorology, ionosphere, and climate and ground global positioning system observations. *Space Weather*. **18**(5): e2019SW002406. Doi: https://doi.org/10.1029/2019SW002406.
24. Maute, A., Richmond, A. D. & Roble, R. G. 2016. Impact of non-migrating tides on the low-latitude ionosphere. *Geophysical Research Letters*. **43**(6): 2423–2432. Doi: https://doi.org/10.1002/2016GL068447
25. Jones, Jr. M., Emmert, J. T., Drob, D. P. & Picone, J. M. 2018. The role of neutral winds in the formation of the winter anomaly. *Journal of Geophysical Research: Space Physics*. **123**(4): 3206–3220. Doi: https://doi.org/10.1002/2017JA024943
26. Fuller-Rowell, T. J. 1996. The "thermospheric spoon": A mechanism for the semiannual density variation. *Journal of Geophysical Research: Space Physics*. **101**(A5): 10727-10735. Doi: https://doi.org/10.1029/95JA03576
27. Matzka, J., O. Bronkalla, K. Tornow, K. Elger. and C. Stolle .2021. Geomagnetic Kp index. *GFZ Data Services*. Doi:10.5880/Kp.0001.
28. Hofmann-Wellenhof, B., Lichtenegger, H. & Collins, J. 1992. Global Positioning System: Theory and practice. Springer-Verlag.
29. Schaer, S. 1999. Mapping and predicting the Earth's ionosphere using the Gobal Positioning System (Publication No. 205). Astronomical Institute, University of Bern.
30. Titheridge, J. F. 1972. The total electron content of the southern midlatitude ionosphere, 1965–1971. *J. Atmos. Terr. Phys*. **35**: 9811001. Doi: https://doi.org/10.1016/0021-9169(73)90077-9.
31. Ghimire, B. D., Chapagain, N. P., Basnet, V., Bhatta, K. & Khadka, B. 2020. Variation of Total Electron Content (TEC) in the quite and disturbed days and their correlation with geomagnetic parameters of Lamjung Station in the year of 2015. *Bibechana*. **17**: 123-132.
32. Pandit, D., Ghimire, B., Amory-Mazaudier, C., Fleury, R., Chapagain, N. P. & Adhikari, B. 2021. Climatology of ionosphere over Nepal based on GPS total electron content data from 2008 to 2018. *Annales Geophysicae*. **39**: 743-758.
33. Richmond, A. D. 1995. Ionospheric electrodynamics using magnetic apex coordinates. *Journal of geomagnetism and geoelectricity*. **47**(2): 191-212.
34. Immel, T. J., Sagawa, E., England, S. L., Henderson, S. B., Hagan, M. E., Mende, S. B. & Paxton, L. J. 2006. Control of equatorial ionospheric morphology by atmospheric tides. *Geophysical Research Letters*. **33**(15). Doi: https://doi.org/10.1029/2006GL026161.
35. Ghimire, B. D., Chapagain, N. P., Basnet, V. & Khadka, B. 2021. Analysis of Tec variations over Nepal obtained from GPS Data on geo-magnetically quiet and disturbed days of the Year 2015. *Journal of Nepal Physical Society*. **7**(2): 102-109.S.
36. Jones, Jr. M., Emmert, J. T., Drob, D. P. & Picone, J. M. 2018. The role of neutral winds in the formation of the winter anomaly. *Journal of Geophysical Research: Space Physics*. **123**(4): 3206–3220. Doi: https://doi.org/10.1002/2017JA024943.
37. Forbes, J. M., Palo, S. E. & Zhang, X. 2008. Solar cycle variability of planetary waves in the mesosphere and lower thermosphere. *Journal of Atmospheric and Solar-Terrestrial Physics*. **70** (11-12): 1621–1629. Doi: https://doi.org/10.1016/j.jastp.2008.06.011.